European Journal of Remote Sensing - 2014, 47: 251-269
doi: 10.5721/EuJRS20144716
Received 21/05/2013, accepted 26/03/2014

European Journal of Remote Sensing
An official journal of the Italian Society of Remote Sensing

www.aitjournal.com

Use of Unmanned Aerial Systems for multispectral survey and tree classification: a test in a park area of northern Italy

Rossana Gini[1]*, Daniele Passoni[2], Livio Pinto[2] and Giovanna Sona[1]

[1]Geomatics Laboratory at Como Campus, DICA, Politecnico di Milano, Como, Italy
[2]DICA, Politecnico di Milano, Milano, Italy
*Corresponding author, e-mail address: rossana.gini@mail.polimi.it

Abstract

In the frame of project FoGLIE (Fruition of Goods and Landscape in Interactive Environment), UAS were used to survey a park area in its less accessible zones, for scenic and stereoscopic videos, 3D modeling and vegetation monitoring. For this last application, specifically, through the acquisition of very high resolution images taken with two UAS-borne compact cameras (RGB and NIR), a DSM of a small vegetated area and the corresponding orthoimages were produced and co-registered. Planimetric and height accuracies in block adjustments and orthophotos are in the range of 0.10 m horizontally and 0.15 m in height. Then, after the derivation of synthetic channels, both unsupervised classification and supervised one were performed in order to test the algorithms' ability to distinguish between different bushes and trees species: some of them were correctly classified by the latter method but misclassifications still remain. The overall accuracy for the unsupervised classification is about 50% while the supervised one yields an overall accuracy around 80%.

Keywords: Classification, DSM, UAS, vegetation , orthophoto, block adjustment.

Introduction: UAS for cultural heritage modelling and park monitoring

Italy is characterized by the presence of many places of both landscape and cultural values, such as museums or areas with heterogeneous and distributed cultural, historical and natural heritage.The management of these areas is complex both from the safeguard point of view and from the fruition one. The latter is mainly realized through paths and exhibition itineraries and the users interfaces consist of fixed stations or audio guides which provide static descriptions of the cultural/natural evidences and are often unsuitable in case of heterogeneous points of interest.

To overcome these limits, the pilot project FoGLIE ("Fruition of Goods Landscape in Interactive Environment") was funded by the local government authority "Regione Lombardia", with the aim of developing an audiovisual movable system and interactive

contents. Visits are made more effective and involving thanks to images, historical documents, virtual tours, 3D videos and models, available in augmented reality visualization by means of advanced devices (e.g. tablets). Furthermore, this innovative guide meets the purpose of enhancing the natural, artistic and cultural heritage and improving the typical land monitoring processes: indeed, it integrates the fruition phase with the documentation and preservation ones thanks to the possibility of recording videos and images automatically referenced in space and time [Gini et al., 2011]. The users can send them to a central system at the Park Main Centre together with explanatory messages: in this way, potential environmental problems can be quickly brought to the attention of the management staff and, at the same time, the simple fruition is turned into active safeguard.

A noteworthy aspect of the project is the use of not conventional aerial platforms, i.e. the so-called "Unmanned Aerial Systems" (UAS): they are "powered aerial vehicles that do not need a human operator physically onboard" [Eisenbeiss, 2009; Eisenbeiss and Sauerbier, 2011]. Depending on their size and on the transportable payload, drones can be equipped with different sensors, including amateur compact cameras, thermal or infrared camera systems or a combination of them [Berni et al., 2009; Nagai et al., 2009; Laliberte et al., 2011; Lucieer et al., 2012].

These new technologies have several advantages with respect to the manned aircraft systems: the low costs, the manoeuvrability, the possibility of being programmed to accomplish flights autonomously or to take very close aerial images and unconventional poses. All these characteristics make UAS the ideal photogrammetric platforms for life-threatening situations or areas which are not reachable by traditional aircrafts [Zhou et al., 2005; Wu et al., 2006; Niethammer et al., 2012]. At the same time, the flights repeatability, the fast data acquisition and its real-time transmission to ground stations (when possible) allow both control of the territory and frequent monitoring. As a consequence, the Unmanned Aerial Systems surely represent a new and flexible technology, able to collect a big amount of very high resolution information for both geometric and descriptive purposes, as generation of Digital Surface Models (DSMs), forest landscape assessment, analysis of critical environmental situations, evaluation of not accessible or not properly enhanced areas and so on.

Within the FoGLIE project, the UAS were used for a double purpose: to carry out indoor and outdoor flights for capturing images suitable for the audiovisual system and to help in the managing of the park territory. The university "Politecnico di Milano" was involved for providing scientific and technical support in the photogrammetric surveys to produce 3D models of some historical buildings and augmented reality scenes, as well as for investigating the potentialities of UAS systems for vegetation monitoring.

In the present paper the attention is focused on a specific part of the project, a pilot survey which aimed at acquiring multispectral UAS images: they were processed with remote sensing classification techniques to detect non native tree species, thereby assisting the Park Forest authority to manage the selective cuttings.

In Section 2 the employed vector-sensors system, the planning and the execution of the UAS survey are described. The high resolution images were geo-referenced separately through a bundle block adjustment (Section 3); afterwards, the RGB data set was used to generate the DSM which, in turn, was employed to create RGB and NIR orthophotos. Both a supervised algorithm and an unsupervised one were run on a layer stack of eight

variables, four original channels plus four synthetic bands (Section 4); eventually, results are discussed in Section 5.

Experiment setup

The FoGLIE project used "Parco Adda Nord" as test area: to the south of Como Lake in Lombardy (Italy), the park follows the course of Adda River, with a narrow and long shape of roughly 55 km. It was selected due to the presence of several elements of both natural and historical value, such as Brivio wetland, the Leonardo's locks and the Crespi d'Adda village, an example of the 19th- and early 20th-century "company town", included into the UNESCO World Heritage List (http://whc.unesco.org/en/list/730/; for more information, please refer to the State of Conservation of World Heritage Properties in Europe [UNESCO, 2006]). Moreover, the park is still rich in native vegetation (see Fig. 1), e.g. alder *(Alnus glutinosa*), plane tree *(Platanus* spp.), poplar *(Populus* spp.), birch *(Betula* spp.), etc. Unfortunately, foreign invasive species were introduced long ago and are now so widespread that periodic selective cuttings are planned in order to protect the local ecosystem: particular care is devoted to tree of heaven *(Ailanthus altissima*), since it spreads like wildfire endangering the local vegetation. Instead the black locust *(Robinia pseudoacacia*) is a non native Italian species now considered naturalized [Celesti-Grapow et al., 2010].

Figure 1 - From left to right: *Alnus glutinosa*, *Ulmus*, *Platanus* and *Robinia Psuedoacacia.*

This work focuses on a pilot experiment on a small area (120x100 m^2, with a difference in altitude of 15 m) located inside the park and close to Medolago village, Bergamo (see Fig. 2).

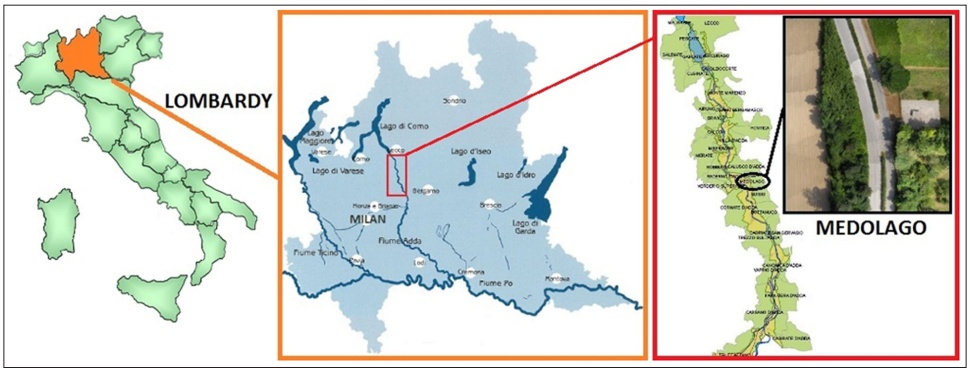

Figure 2 - Location of the survey area.

Selected together with the "Parco Adda Nord" technical staff, it comprehends several land cover types, i.e. a small building, an agricultural field, a road and different tree species: an extended scrub of tree of heaven (*Ailanthus altissima*), hornbeam (*Carpinus betulus*), elm (*Ulmus* spp.) and black locust (*Robinia pseudoacacia*).

The vector-sensor system

The employed platform was the quadrirotor Microdrones™ MD4-200 owned by Zenit S.r.l.: characterized by vertical take-off and landing, this vehicle can fly by remote control or autonomously, using the automatic pilot function and a GPS navigation system. Moreover, the MD4-200 is furnished with a software package which allows the user to manage all the functions needed to plan, monitor and analyze the flight (see Tab. 1 for more details).

Table 1 - Some technical specifications of MD4-200.

Payload capacity	Up to 200 g
Flight duration	~ 30 min
Flight radius	max. 500 m
Flight altitude	max. 150 m

The digital compact camera, selected for taking RGB images, was the Pentax Optio A40 due to its dimensions and low weight (130 g) which make it ideal to be carried by the MD4-200. It features a CCD image sensor and, with an actual resolution of 12 megapixels, it can take photos with 4000x3000 pixels as maximum resolution. The second digital compact camera was a Sigma DP1, furnished with a Foveon X3 sensor and specifically modified by the owner (Zenit S.r.l. - the same of the Pentax) to allow the recording of near infrared radiation [Alba et al., 2011].

In order to reduce the Sigma's weight (250 g), the camera was directly connected to the MD4-200 battery, thereby shortening the autonomy of the latter. Further cameras details are reported in Table 2.

Table 2 - Some technical specifications of the cameras.

	Pentax Optio A40	Sigma DP1
Focal length (mm)	7.90 (fixed)	16.60 (fixed)
Sensor (mm)	7.48 x 5.61	20.70 x 13.60
Sensor (px)	4000 x 3000	2650 x 1740
Pixel size (μm)	1.87	7.81

UAS survey planning and data acquisition

Because of the MD4-200 low payload, the concurrent use of the cameras was not possible thus only one at a time was employed: this required the development of a subsequent co-registration procedure in order to work with multispectral information for the vegetation classification [Nebiker et al., 2008].

To cover the entire area, it was necessary to plan the acquisition of three strips (see Fig. 3); moreover, the flight height was kept constant at roughly 55 m due to security issues, thereby determining different Ground Sample Distances (GSD), equal to 1.33 cm for the Pentax and 2.63 cm for the Sigma DP1. The UAS flew autonomously on the testing area thanks to

the automatic pilot function, while the take-off and the landing were remotely controlled by the operator.

Figure 3 - Flight plan: strips and RGB camera projection centers.

Data were acquired in a sunny day of July 2011, by performing six separate flights in the South-North direction: indeed, the low UAS flight range (approximately up to 20 minutes) entailed the need to perform a single flight for each strip, by setting down the MD4-200 and changing its battery. For what concerns the RGB dataset, the overall result was satisfactory although the attitude of some images was not nadiral, probably because of the presence of breeze or wind at the flight height. Instead, regarding the NIR data, several images were blurred and this problem might be linked to the long exposure time, chosen in order to capture infrared wavelengths. Another aspect to be underlined but concerning both images sets is that the illumination was not uniform within the single block, due to the time elapsed between the first and the third strips of each of them.
In conclusion, the procedure described in this paper was applied to 35 RGB images and 19 NIR ones, selected from the original datasets of 43 and 40 photos respectively, on the basis of two criteria: maintaining an overlap as homogeneous as possible throughout the block and maximizing the number of visible ground surveyed points.

Block adjustment and surface modeling

In order to calibrate the cameras, a b/w standard square panel was used, with a printed pattern of signals that are automatically recognized by PhotoModeler 6 (by Eos System Inc. http://www.photomodeler.com/index.html): a set of images in suitable positions and

orientation were acquired by both cameras and then employed by the software to compute the parameters of a Brown model [Brown, 1971], summarized in Table 3.

Table 3 - Calibration parameters estimated by PhotoModeler 6.

	Pentax Optio A40	Sigma DP1
Theoretical Focal Length (mm)	7.90	16.60
Calibrated Focal Length (mm)	8.0968	16.8763
Principal Point x_p (mm)	3.6031	10.3560
Principal Point y_p (mm)	2.7577	6.9976
Radial Distortion k_1	$2.900 \cdot 10^{-3}$	$2.639 \cdot 10^{-4}$
Radial Distortion k_2	$-1.205 \cdot 10^{-5}$	$-7.068 \cdot 10^{-7}$
Decentering Distortion p_1	$-2.955 \cdot 10^{-5}$	$-6.106 \cdot 10^{-5}$
Decentering Distortion p_2	$-3.432 \cdot 10^{-4}$	$5.519 \cdot 10^{-5}$

After this preliminary step, the RGB images were processed in a bundle block adjustment [Ackermann and Tsingas, 1994] in PhotoModeler 6 with 16 GCPs, 13 Check Points (CPs) and 218 Tie Points (TPs) manually selected; this set of TPs was then exported and used also in LPS 2011 (Leica Photogrammetry Suite, ERDAS IMAGINE by Intergraph http://geospatial.intergraph.com), in order to compare the results coming from close range and aerial photogrammetric software packages.
The residuals on ground coordinates of CPs were analyzed: even if accuracies are of the order of centimeters in both cases, better results came from LPS regarding the height coordinate (see Tab. 4).

Table 4 - Statistics of CPs residuals (m).

	PhotoModeler			LPS		
	ΔE	ΔN	Δh	ΔE	ΔN	Δh
Mean	0.034	-0.017	0.121	0.018	-0.043	0.037
Std. Dev.	0.034	0.036	0.090	0.047	0.071	0.082
RMSE	0.047	0.038	0.149	0.048	0.081	0.087

Furthermore, the differences between the Exterior Orientation parameters (EO) estimated by PhotoModeler (PM) and the ones from LPS were computed, by showing variations up to some decimeters but always below 1 m (Tab. 5).

Table 5 - Statistics of differences in EO parameters (lengths in meters, angles in degrees).

	EO_{PM} - EO_{LPS}					
	ΔE	ΔN	Δh	Δω	Δϕ	Δκ
Mean	0.417	0.289	-0.058	0.313	0.554	0.064
Std. Dev.	0.085	0.076	0.188	0.079	0.057	0.176
Max	0.682	0.491	0.339	0.468	0.675	0.423
Min	0.297	0.159	-0.355	0.139	0.458	-0.197

In the following table (Tab. 6), the accuracies of the EO parameters only from LPS are listed, since PhotoModeler does not compute them.

Table 6 - Accuracies of EO parameters from LPS (lengths in meters, angles in degrees).

	Accuracies EO_{LPS}					
	E	N	h	ω	ϕ	κ
Mean	0.081	0.082	0.030	0.092	0.088	0.020
Std. Dev.	0.052	0.047	0.019	0.050	0.053	0.009

Lastly, the Exterior Orientation parameters were compared to the UAS position and attitude data, registered during the flight by the low-cost navigation system on board. As expected, these measurements can be considered only a rough approximation of the actual camera projection centers: indeed the position acquired by GPS code and the attitude obtained by low cost IMU were affected by errors not acceptable for photogrammetric purposes. The EO parameters estimated both by PhotoModeler and LPS departed appreciably from the recorded values, as expected, due to the low accuracies of the positioning system (see Tab. 7).

Table 7 - Statistics of differences between EO parameters from software packages and those from onboard sensor (lengths in meters, angles in degrees).

	EO_{LPS} - $EO_{GPS/IMU}$					
	ΔE	ΔN	Δh	Δω	Δϕ	Δκ
Mean	0.02	-0.28	1.88	0.527	-2.009	4.776
Std. Dev.	0.48	1.64	0.82	7.062	1.687	4.769
Max	1.25	6.49	4.19	12.561	1.731	13.675
Min	-0.97	-2.08	0.31	-6.849	-4.864	-7.148
	EO_{PM} - $EO_{GPS/IMU}$					
	ΔE	ΔN	Δh	Δω	Δϕ	Δκ
Mean	0.18	0.16	1.80	0.559	-1.747	4.703
Std. Dev.	0.58	1.82	0.82	7.171	1.902	4.713
Max	1.55	7.73	4.27	13.159	2.674	13.664
Min	-1.09	-1.46	0.22	-7.398	-4.818	-7.271

PhotoModeler and LPS yielded similar results with the highest differences in N (along strip axis) and ω, thus making clear it is not possible to obtain an accurate position of the camera by the onboard navigation system [Gini et al., 2012].
The bundle block adjustment algorithm of LPS 2011 was separately run also on the NIR images; then the attention was focused on the co-registration of the two datasets, necessary to work with multispectral images.

The DSM generation

Thanks to the modulus of Automatic Terrain Extraction (ATE) of LPS, a Digital Surface Model (DSM) was created by using the oriented block of RGB images with a high ground resolution of 0.10x0.10 m^2.The automatic generation of the DSM starts from the extraction of homologous points on pairs of images, by exploiting the epipolar geometry and by computing the cross-correlation coefficient between the two images ("patch" and "slave"). Tests are then performed to eliminate any possible outliers. Once the images' exterior orientation is known, the ground coordinates of the points are computed for space forward intersection (http://geospatial.intergraph.com).

The comparison with the 37 ground surveyed points yielded the statistics in Table 8.

Table 8 - Accuracies of 37 height values: DSM compared with GPS heights (m).

	$h_{DSM} - h_{GPS}$
Mean	0.054
Std. Dev.	0.141
Max	0.436
Min	-0.305
RMSE	0.151

Beyond outliers near the borders, it is possible to highlight the presence of isolated spikes in the vegetation whose canopy, nevertheless, is generally quite well modeled. A wrong interpolation can be found in the middle of the road (see Fig. 4), where the presence of gravel maybe prevented the algorithm from modeling a flat surface, like actually it is. Therefore only few edits were required with respect to the purpose, i.e. the vegetation classification.

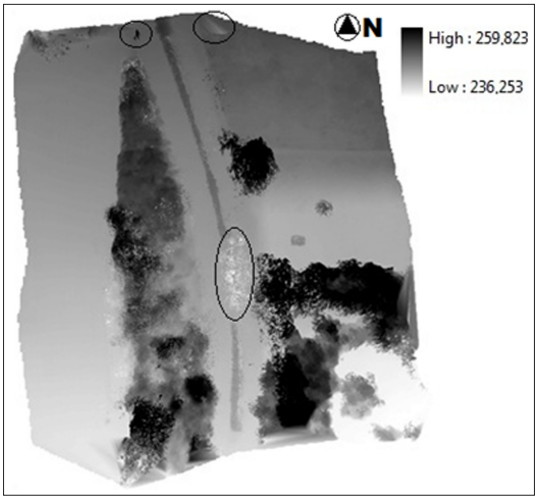

Figure 4 - DSM of the test area and, in the circles, some wrong interpolations (heights in m a.s.l.).

Orthophotos and mosaicking

Once a DSM was available, 35 RGB and 19 NIR separate orthophotos were generated from the original images, with ground resolution of 0.05x0.05 m^2, and mosaicked separately thanks to the proper tool of LPS: even if it is able to create seam lines automatically, a manual correction was needed to minimize as much as possible any sharp illumination changes between images and strips. At the end the two overall orthophotos (RGB and NIR, see Fig. 5), co-registered through the projection on the same DSM, were resized for having equal extension of roughly 100x85 m^2 (1982x1687 pixels).

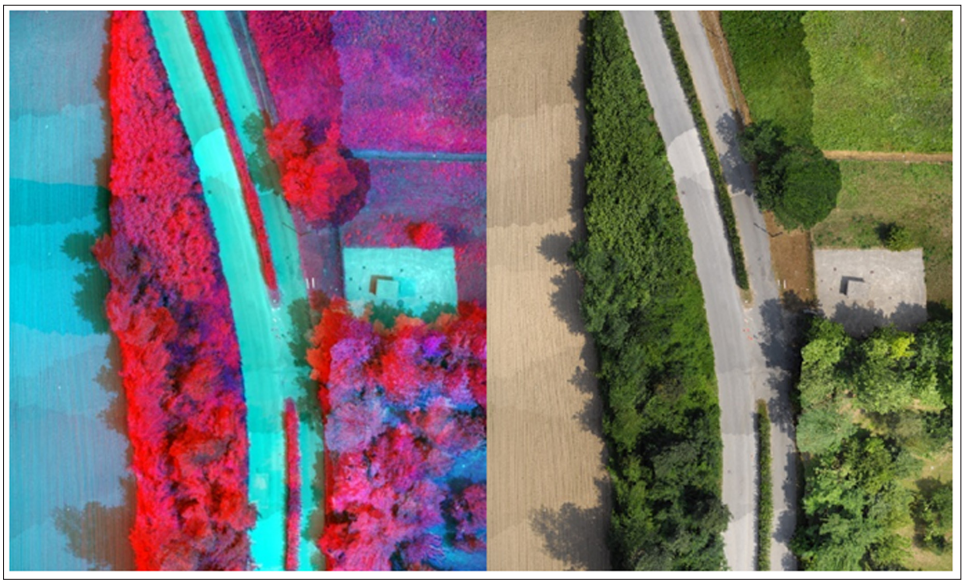

Figure 5 - Color Infra Red (CIR) and RGB orthophotos after co-registration.

Separate differences for the two orthophotos were computed by using 37 ground surveyed points, excluding few non visible points (12 in RGB and 5 in IR): some small differences remain in horizontal positions due to the distinct block adjustments (Tab. 9).

Table 9 - Statistics of the planimetric differences of orthophotos with respect to ground surveyed points (m).

	RGB-GPS	IR-GPS
Mean	0.086	0.065
Std. Dev.	0.053	0.037
Max	0.190	0.175
Min	0.009	0.016
RMSE	0.101	0.075

Moreover, by comparing coordinates of 25 ground control points visible on both orthophotos, the co-registration statistics of the differences can be checked (Tab. 10).

Table10 - Statistics of differences between orthophotos (m).

	RGB-IR
Mean	0.076
Std. Dev.	0.035
Max	0.136
Min	0.026
RMSE	0.084

Analysis of vegetation

Starting from the original 4 layers (Red, Green, Blue and NIR), several types of input quantities - let's call them "variables" - were derived in order to improve the tree species' classification, as already done in previous experiences [Gini, 2010]. In the context of this pilot experiment, a first quick procedure was carried out by computing typical indices (as NDVI) or by doing operations like band ratios, both present in literature for a long time [Silleos et al., 2006]. Only radiometric variables were created since the geometrical ones (such as curvature, slope, aspect and so on) do not seem to have a crucial role in classifying trees species, unless these latter have a characteristic and well-defined shape (e.g. cypress) or a particular limited height: this is not completely true for the species of interest. At the moment, it is in progress the analysis of the variables related to textural features because at least one of the species, i.e. tree of heaven (*Ailanthus altissima*), might be easily distinguishable by the structure of the leaves (as visible in Fig. 6).

Figure 6 - Leaves of tree of heaven (*Ailanthus altissima*).

Thus, the following spectral variables were generated in ERDAS Imagine:

a) NDVI: the Normalized Difference Vegetation Index is quite powerful in performing a qualitative classification thanks to its capacity to distinguish alive vegetated areas from other surface types (water, soil, etc.). It is expressed as the difference between the NIR and the red bands normalized by the sum of these [Silleos et al., 2006];
b) Green ratio: it is obtained by dividing the green layer by the sum of all the four bands as done in previous experiences [Gini, 2010];
c) IHS: it is possible to define a color space that uses Intensity (brightness), Hue (dominant color) and Saturation (color's purity) as the three positional parameters in place of R, G, B. After the transformation, the three parameters were separated and only Hue and Saturation were employed: indeed they are connected to the

spectral characteristics of the surface, whereas the intensity is mainly related to the characteristics which are common to the three original layers (RGB), as the topography [Brivio et al., 2006].

Since the computation of these variables from original channels influenced both the values range and the data type, it was necessary to uniform them to a common unsigned 8 bit (0-255): it was performed by employing the "rescale" function implemented in ERDAS, that stretches or compresses the data to meet the new interval. This operation of rescaling was necessary to stack the 8 variables (the 4 derived and the original 4 layers) and to save them as a single file with 8 layers.
Since the classification was performed also with a standard supervised algorithm, it was necessary to have the ground position of samples belonging to the different classes: in remote sensing, it is usually performed a ground sampling of the involved spectral signatures through a spectrophotometer and a radiometric correction and calibration of the images. However, for the project's purposes, the attention was focused on the development of empirical procedures based on quick surveys: hence the training and validation samples were selected directly on images and generated on the basis of GPS surveyed positions of some trees as well as the photographic and handwritten documentation collected with the park staff. In this case, the number of classes were chosen not only on the basis of the land covers and tree species really present in the area, but also on the fact that they had to be clearly visible in the orthophotos. Phytolacca (*Phytolacca* spp.), for instance, is a non native shrub certainly present and recognizable on the ground, but not on the images since it is often covered by the crowns of higher trees. Therefore, it was decided to select 8 classes with four belonging to tree species, listed in Figure 7 together with the samples.

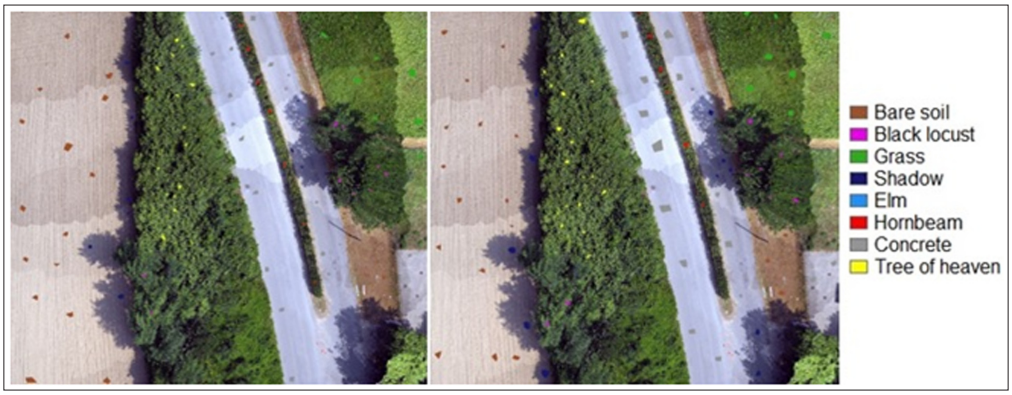

Figure 7 - Training samples (on the left) and validation samples (on the right).

Unsupervised classification: ISODATA

The so-generated layer stack was classified in 8 land cover types by means of a classic unsupervised algorithm, the ISODATA [Tou and Gonzalez, 1974] implemented in ERDAS Imagine (Fig. 8).

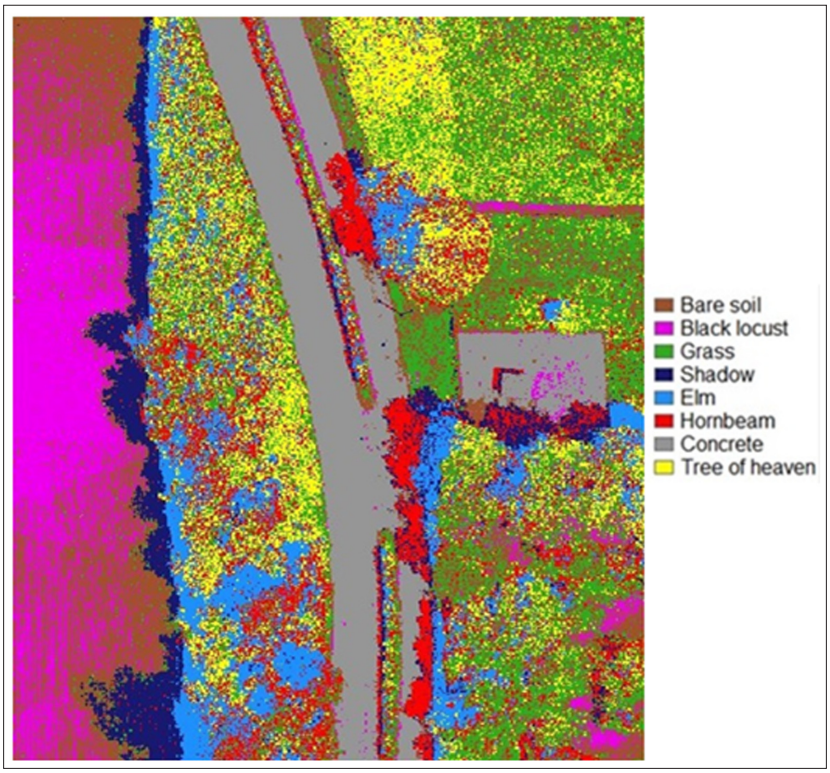

Figure 8 - Unsupervised classification (8 classes).

It can be noted that only the classes with deeply different spectral signatures were recognized and separated (for instance the concrete), while the algorithm mixed all the classes belonging to similar land cover. Thus, the 4 classes assigned to the vegetation are widespread and mixed and they do not correspond to separate tree species: for instance, the scrub of tree of heaven (*Ailanthus altissima*) in the upper part, the isolated black locust (*Robinia pseudoacacia*) in the grass, the plane trees (*Platanus* spp.) near the small house are misclassified. Furthermore, it can be noted that the shadowed areas were not recognized as a single class but were divided into three different ones (blue, red and light blue). Anyway, such a classification can be useful in the preliminary analysis of the spectral characteristics of the image: this step is often done before applying a supervised classification [Brivio et al., 2006].

The assessment of an unsupervised classification, which does not use any training samples, depends of course on "a posteriori" definition of classes on the basis of visual interpretation. By assigning to the resulting classes a prevalent meaning, the quality of the classification can be evaluated through the error matrix (see Tab. 11), which shows how many pixels of each class were actually classified into each class. The error matrix is very useful not only to estimate the amount of misclassified pixels but also to understand between which classes the misclassification occurs more frequently: a good classification is characterized by high values on the diagonal and low values out of it [Congalton, 1991].

Table 11 - Error matrix of Isodata classification.

ISODATA - ERROR MATRIX									
CLASS → / VAL. SAMPLES ↓	Tree of heaven	Horn beam	Elm	Black locust	Concrete	Grass	Bare soil	Shadow	# Pixel of val. samples
Tree of heaven	**261**	249	11	451	0	1267	2	1	2242
Hornbeam	74	**255**	537	344	0	201	1	878	2290
Elm	12	53	**96**	68	0	39	0	149	417
Black locust	0	0	0	**3**	39	64	3094	0	3200
Concrete	0	0	1	0	**4097**	0	2	0	4100
Grass	425	391	216	672	0	**2706**	295	5	4710
Bare soil	21	19	47	223	0	909	**2234**	9	3462
Shadow	0	1	7	0	0	1	0	**1160**	1169
# Pixel of class	793	968	915	1761	4136	5187	5628	2202	21590

An overall accuracy is calculated from this matrix by taking the sum of the elements on the diagonal and dividing this by the total number of pixels. Traditionally, the total number of correct pixels in a category is divided by the total amount of pixels of that category as derived from the reference data: this number indicates the probability of a reference pixel being correctly classified and is often called "producer's accuracy" (PA). On the other hand, if the total number of correct pixels in a category is divided by the total number of pixels that were classified in that category (i.e. the row total), then this result is indicative of the probability that a pixel classified on the map/image actually represents that category on the ground ("user's accuracy", UA) [Story and Congalton, 1986]. Another statistic which can be generated from the error matrix is the Kappa coefficient (Tab. 12): it takes into account all the values in the matrix and indicates how much of an improvement there is compared to randomly allocating pixels to classes [Congalton and Green, 2008; Murray et al., 2010].

Table 12 - Accuracies of Isodata classification.

	UA	PA
Tree of heaven	11.64%	31.40%
Hornbeam	11.14%	26.34%
Elm	23.02%	10.49%
Black locust	0.09%	0.17%
Concrete	99.93%	99.06%
Grass	57.45%	52.17%
Bare soil	64.53%	39.70%
Shadow	99.23%	52.70%

Overall Classif. Accuracy	50.08%
Kappa	0.4074

Supervised classification: Maximum Likelihood

A second test was performed by running a standard supervised algorithm, which required the use of training samples; on the layer stack already used in the unsupervised classification, the Maximum Likelihood algorithm was run in ERDAS Imagine (see Fig. 9): visually, it is possible to note how the tree of heaven was partly identified (the scrub in the upper left part of the image), even if several pixels of the grass were assigned to this class too.

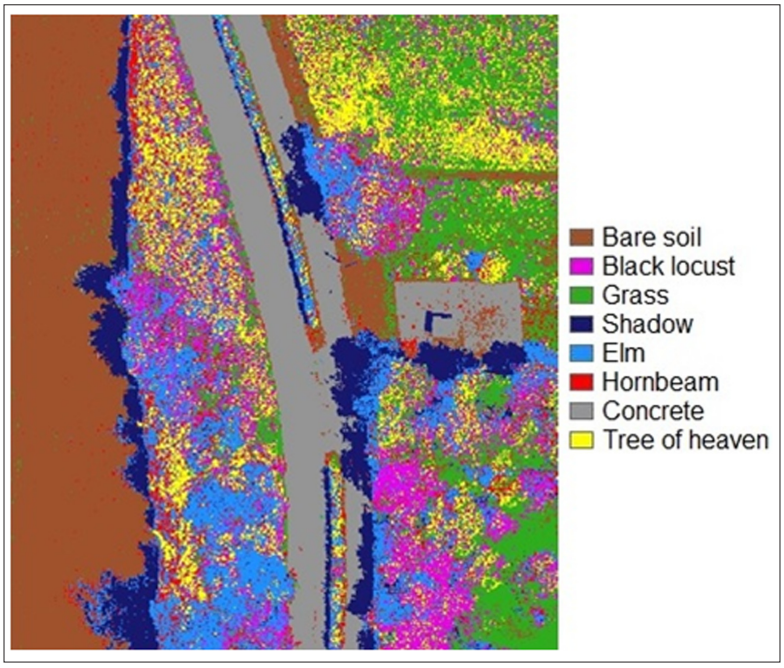

Figure 9 - Supervised classification (8 classes).

The quality of classification has been evaluated again through the error matrix and the producer's, user's and overall accuracies (see Tab. 13 and Tab.14).

Compared with the unsupervised classification, this second one yields, as expected, higher values of accuracies in terms of overall accuracy, K value and for most of the user's and producer's accuracies.

From a detailed analysis of the error matrix it is evident that, a part for the classes of non vegetated soil (concrete, bare soil, shadow), among green coverages only elm is sufficiently separated (PA 76%); tree of heaven and black locust are assigned with a high percentage to the right classes (66% and 50% respectively), but are partially mixed also with grass sample pixels. The worst case is hornbeam, that is totally misclassified and attributed 43% to tree of heaven, 30% to elm, 13% to grass and only 10% to the proper hornbeam class. Thus, the non native species which the attention was focused on, i.e. the tree of heaven, is not assigned to other classes but, unfortunately, is "compromised" by the erroneous attribution of pixels which belong to the black locust, the hornbeam and the grass (the tree of heaven UA is in fact only 20%).

Table 13 - Error matrix of Max. Likelihood classification.

MAXIMUM LIKELIHOOD - ERROR MATRIX									
CLASS → / VAL. SAMPLES ↓	Tree of heaven	Horn beam	Elm	Black locust	Concrete	Grass	Bare soil	Shadow	# Pixel of val. samples
Tree of heaven	**528**	417	39	552	0	1110	0	0	2646
Hornbeam	29	**101**	33	60	9	145	28	36	441
Elm	14	283	**695**	121	1	70	0	154	1338
Black locust	179	40	119	**880**	0	509	0	23	1750
Concrete	0	0	0	0	**4103**	0	1	5	4109
Grass	43	126	14	148	0	**3310**	47	85	3773
Bare soil	0	0	0	0	23	41	**5552**	0	5616
Shadow	0	1	15	0	0	2	0	**1899**	1917
# Pixel of class	793	968	915	1761	4136	5187	5628	2202	21590

Table 14 - Accuracies of Max. Likelihood classification.

	UA	PA
Tree of heaven	19.95%	66.58%
Hornbeam	22.90%	10.43%
Elm	51.94%	75.96%
Black locust	50.29%	49.97%
Concrete	99.85%	99.20%
Grass	87.73%	63.81%
Bare soil	98.86%	98.6%
Shadow	99.06%	86.2%

Overall Classif. Accuracy	79.06%
Kappa	0.7477

In conclusion, the supervised classification gives better results : the overall accuracy is 50% higher than the unsupervised one.

Discussion of results

Generally speaking, the results cannot be considered completely satisfactory, even if it was expected that not all the tree species were immediately distinguished. However, the experiment revealed the system capabilities: first of all, such a proximal sensing survey can be useful for generating a DSM and, consequently, a Canopy Height Model which can enable the estimation of dendrometric parameters and typological-structural characteristics in small scenarios [Hall et al., 2003]. Moreover, obviously depending on the case study, the use of traditional indexes, in the context of a new application at very high geometric resolution, can produce a subdivision into species groupings that contain enough information to distinguish specific tree species. The use of complementary data can help: for instance, where the tree of heaven was confused with the grass, the problem can be solved by using

also the height of the vegetation, easily obtainable from the DSM [Naidoo et al., 2012].
Lastly the geometric accuracies, achievable after the block orientation, were determined: in particular, the great distortions of compact cameras and the anomalies in the images' orientations worsened the restitution accuracies with respect to those of traditional photogrammetric flights, even if a standard calibration procedure is applied. On the other hand, these issues were sufficiently compensated by the very high geometrical resolution, since this kind of application does not require an accuracy at centimeter level, unlike other close-range surveys (e.g. for architectural and restoration purposes); in this sense, also inaccuracies of some pixels can be disregarded.
In this respect, it is necessary to be careful in not exaggerating in geometric resolution, by fine-tuning the flight heights and, consequently, the GSD: otherwise, it can happen that the huge amount of data slows down the process and worsens the system performance, without adding information useful to improve the classification.
Another issue, related to the flight planning and to the vector-sensor system, is the great number of images: they needed to be mosaicked and this required the operator's intervention in a demanding and time consuming process to produce an overall orthoimage of a very small area (100x85 m^2). Thus the workflow should be automated as much as possible through the implementation of algorithms specifically designed for processing UAS images [Barazzetti et al., 2010; Remondino et al., 2011].
Another aspect to remember is the UAS low autonomy, which entailed the need to perform a single flight for each strip, by setting down the MD4-200 and changing its battery: thus, the illumination was not uniform within the single block of images, because of the time elapsed between the first and the third strip. A single flight should allow the overcoming of these limits: indeed it would reduce the presence of radiometric jumps, which can affect the creation of empirical "spectral signatures" and their effectiveness, as probably happened in the case study although the samples were selected on the entire orthoimage. Certainly, another aspect played a main role in this step and it is the low number of channels: the Red, Green, Blue and NIR ones provided a limited radiometric resolution which did not allow a completely effective classification of the tree species.
The solution of this problem can be found in the selection of proper multispectral or hyperspectral cameras which, at the same time, would allow to work with already co-registered images: unfortunately, UAS are usually able to carry a limited payload and, since they are new emerging aerial platforms, there are not so many miniaturized multispectral cameras on the market. Anyway, those available, like Tetracam ADCLite, have lower geometric resolution and smaller sensor's dimension (e.g. 5.99 mm x 4.5 mm), thus yielding very small single image ground print (roughly 45 m x 35 m) and increasing the number of photos necessary to cover the same extension. Not to mention the hyperspectral sensors, capable of collecting suitable spectral data but characterized by great weight (hence, bigger vehicles are necessary) and higher costs (even hundred of k€ as Specim V10 or V16 systems, www.specim.fi).

Conclusions

In this paper an UAS survey was described in details, that is, from the flight planning to the acquired data processing, which was performed with the specific aim of classifying vegetation. It has been proved that through UAS is possible to realize local multispectral

surveys and subsequent high quality analysis. As a light multispectral camera was not available, two separate surveys were done, producing two orthophotos coregistered in a second time on the same DSM. Height and planimetric distances between RGB and NIR orthophotos, computed on several ground control points surveyed by GPS, show a good quality and coherence of the two products of the order of few GSD (0.10 m horizontally; 0.15 m in height). Moreover, it has been proved that it is possible, with low cost instruments, to obtain a classification of different vegetable species that can help in identifying specific variety: the Maximum Likelihood algorithm yielded an overall classification accuracy about 80%, with producer's accuracy values higher than 90% for shadow, concrete and bare soil, and a value of 66% for the tree of heaven.

Nevertheless the results are not completely satisfactory and the experiment revealed system capabilities and limits: besides the workflow that could be optimized and partially automated, different survey planning should be tested on wider areas and at higher elevations, even if with a lower geometric resolution. For what concerns the sensors, multispectral and hyperspectral cameras are certainly more suitable for classification purposes, but their use is constrained by the UAS limited payload and by the current high costs.

Eventually, the classification outcomes could be improved by deriving new textural variables, depending on the characteristics of the trees' species of interest (e.g. tree of heaven). Further efforts might be addressed in achieving a more effective classification through the spectral signatures collection at various periods of the year as well as on plants at different phenological development phase and vegetative states of health. Of course, this procedure operates in the opposite direction with respect to the demands of a quick and low cost monitoring: a careful analysis of cost/benefit is needed according to each survey's requirements.

Acknowledgements

The authors thank the company Zenith S.r.l for the UAS flights and the reviewers for their careful reading of the paper and for the comments which helped to improve it.

The project FoGLIE (Fruition of goods landscape in interactive environment) was sponsored by Regione Lombardia (project id 14508030).

References

Ackermann F., Tsingas V. (1994) - *Automatic Digital Aerial Triangulation*. In: Proceedings of the American Society for Photogrammetry and Remote Sensing, Annual Convention, Reno, pp. 1-12.

Alba M., Barazzetti L., Giussani A., Roncoroni F., Scaioni M. (2011) - *Filtering vegetation from terrestrial point clouds with low-cost near infrared cameras*. Italian Journal of Remote Sensing, 43: 55-75. doi: http://dx.doi.org/10.5721/ItJRS20114325.

Barazzetti L., Remondino F., Scaioni M. (2010) - *Fully automated UAV image-based sensor orientation*. International Archives of the Photogrammetry, Remote Sensing and Spatial Information Sciences, 38 (1). Calgary, Canada (on CD-ROM).

Berni J.A.J., Zarco-Tejada P.J., Suárez L., Fereres E. (2009) - *Thermal and narrowband multispectral remote sensing for vegetation monitoring from an Unmanned Aerial Vehicle*. IEEE Transactions on Geoscience and Remote Sensing, 47 (3): 722-738. doi:

http://dx.doi.org/10.1109/TGRS.2008.2010457.

Brivio P.A., Lechi G., Zilioli E. (2006) - *Principi e metodi di Telerilevamento*. CittàStudi (Eds), Utet, Torino, pp. 525. ISBN: 88-251-7293-1.

Brown D.C. (1971) - *Close-Range Camera Calibration.* Photogrammetric Engineering, 37 (8): 855-866.

Celesti-Grapow L., Alessandrini A., Arrigoni P.V., Assini S., Banfi E., Barni E., Bovio M., Brundu G., Cagiotti M.R., Camarda I., Carli E., Conti F., Del Guacchio E., Domina G., Fascetti S., Galasso G., Gubellini L., Lucchese F., Medagli P., Passalacqua N.G., Peccenini S., Poldini L., Pretto F., Prosser F., Vidali M., Viegi L., Villani M.C., Wilhalm T., Blasi C. (2010) - *Non-native flora of Italy: Species distribution and threats*. Plant Biosystems, 144 (1): 12-28. doi: http://dx.doi.org/10.1080/11263500903431870.

Congalton R.G. (1991) - *A review of assessing the accuracy of classifications of remotely sensed data*. Remote Sensing of Environment, 37: 35-46. doi: http://dx.doi.org/10.1016/0034-4257(91)90048-B.

Congalton R.G., Green K. (2008) - *Assessing the accuracy of remotely sensed data: principles and practices*. Taylor & Francis Group, Boca Raton, pp. 180. doi: http://dx.doi.org/10.1201/9781420055139.

Eisenbeiss H. (2009) - *UAV Photogrammetry*. Ph.D. thesis, Diss. ETH N. 18515. Institute of Geodesy and Photogrammetry, ETH Zürich, Switzerland, pp. 235.

Eisenbeiss H., Sauerbier M. (2011) - *Investigation of UAV systems and flight modes for photogrammetric applications*. The Photogrammetric Record, 26: 400-421. doi: http://dx.doi.org/10.1111/j.1477-9730.2011.00657.x.

Gini R. (2010) - *Processing of high resolution and multispectral aerial images for forest DSM production and tree classification*. Master thesis, DIIAR, Politecnico di Milano, Italy, pp. 145.

Gini R., Passoni D., Pinto L., Sona G. (2011) - *Utilizzo di droni per la documentazione e la valorizzazione dei beni paesaggistici: il progetto FoGLIE*. Atti 15a Conferenza Nazionale ASITA. Reggia di Colorno, pp. 1195-1203.

Gini R., Passoni D., Pinto L., Sona G. (2012) - *Aerial images from an UAV system: 3D modeling and tree species classification in a park area*. International Archives of the Photogrammetry, Remote Sensing and Spatial Information Sciences, XXXIX (B1): 361-366. doi: http://dx.doi.org/10.5194/isprsarchives-XXXIX-B1-361-2012.

Hall A., Louis J., Lamb D. (2003) - *Characterising and mapping vineyard canopy using high-spatial-resolution aerial multispectral images*. Computers & Geosciences, 29: 813-822. doi: http://dx.doi.org/10.1016/S0098-3004(03)00082-7.

Laliberte A.S., Goforth M.A., Steele C.M., Rango A. (2011) - *Multispectral remote sensing from Unmanned Aircraft: image processing workflows and applications for rangeland environments*. Remote Sensing, 3: 2529-2551. doi: http://dx.doi.org/10.3390/rs3112529.

Lucieer A., Robinson S., Turner D., Harwin S., Kelcey J. (2012) - *Using a micro-UAV for ultra-high resolution multi-sensor observations of Antarctic moss beds*. International Archives of the Photogrammetry, Remote Sensing and Spatial Information Sciences, XXXIX (B1): 429-433. doi: http://dx.doi.org/10.5194/isprsarchives-XXXIX-B1-429-2012.

Murray H., Lucieer A., Williams R. (2010) - *Texture-based classification of sub-*

antarctic vegetation communities on Heard Island. International Journal of Applied Earth Observation and Geoinformation, 12: 138-149. doi: http://dx.doi.org/10.1016/j.jag.2010.01.006.

Nagai M., Chen T., Shibasaki R., Kumagai H., Ahmed A. (2009) - *UAV-Borne 3-D mapping system by multisensor integration*. IEEE Transactions on Geoscience and Remote Sensing, 47 (3): 701-708. doi: http://dx.doi.org/10.1109/TGRS.2008.2010314.

Naidoo L., Cho M.A., Mathieu R., Asner G. (2012) - *Classification of savanna tree species, in the Greater Kruger National Park region, by integrating hyperspectral and LiDAR data in a Random Forest data mining environment*. ISPRS Journal of Photogrammetry and Remote Sensing, 69: 167-179. doi: http://dx.doi.org/10.1016/j.isprsjprs.2012.03.005.

Nebiker S., Annen A., Scherrer M., Oesch D. (2008) - *A light weight multispectral sensor for micro UAV - opportunities for every high resolution airborne remote sensing*. International Archives of the Photogrammetry, Remote Sensing and Spatial Information Sciences, XXXVII(B1): 1193-1199.

Niethammer U., James M.R., Rothmund S., Travelletti J., Joswig M. (2012) - *UAV-based remote sensing of the Super-Sauze landslide: evaluation and results*. Engineering Geology, 128: 2-11. doi: http://dx.doi.org/10.1016/j.enggeo.2011.03.012.

Remondino F., Barazzetti L., Nex F., Scaioni M., Sarazzi D. (2011) - *UAV photogrammetry for mapping and 3D modeling - current status and future perspectives*. International Archives of the Photogrammetry, Remote Sensing and Spatial Information Sciences, XXXVIII-1(C22): 25-31. doi: http://dx.doi.org/10.5194/isprsarchives-XXXVIII-1-C22-25-2011.

Silleos G.N., Alexandridis T.K., Gitas I.Z., Perakis K. (2006) - *Vegetation Indices: advances made in biomass estimation and vegetation monitoring in the last 30 years*. Geocarto International, 21 (4): 21-28. doi: http://dx.doi.org/10.1080/10106040608542399.

Story M., Congalton R. (1986) - *Accuracy assessment: a user's perspective*. Photogrammetric Engineering and Remote Sensing, 52 (3): 397-399.

Tou J.T., Gonzalez R.C. (1974) - *Pattern Recognition Principles*. Addison-Wesley Publishing Company, New York. pp. 377. doi: http://dx.doi.org/10.1002/zamm.19770570626.

UNESCO (2006) - *State of Conservation of World Heritage Properties in Europe. Crespi d'Adda, Italy*. Periodic Reporting, Section II, pp. 4.

Wu J., Zhou G. (2006) - *High-resolution planimetric mapping from UAV video for quick-response to natural disaster*. IEEE International Geoscience and Remote Sensing Symposium (IGARSS), pp. 3316-3319. doi: http://dx.doi.org/10.1109/IGARSS.2006.856.

Zhou G., Li C., Cheng P. (2005) - *Unmanned Aerial Vehicle (UAV) real-time video registration for forest fire monitoring*. IEEE International Geoscience and Remote Sensing Symposium (IGARSS), pp. 1803 - 1806. doi**:** http://dx.doi.org/10.1109/IGARSS.2005.1526355.